LANGMUIR

Interface Components: Nanoparticles, Colloids, Emulsions, Surfactants, Proteins, Polymers

Set of Highly Stable Amine- and Carboxylate-terminated Dendronized Au Nanoparticles with Dense Coating and Nontoxic Mixed-dendronized Form

Arunendra Saha Ray, William Emmanuel Ghann, Phoebe Sisoen Tsoi, Brian Szychowski, Lance T. Dockery, Yewon Joanna Pak, Wenjing Li, Maureen A Kane, Peter W Swaan, and Marie Christine Daniel

Langmuir, **Just Accepted Manuscript** • DOI: 10.1021/acs.langmuir.8b03196 • Publication Date (Web): 04 Feb 2019

Set of Highly Stable Amine- and Carboxylate-terminated Dendronized Au Nanoparticles with Dense Coating and Nontoxic Mixed-dendronized Form

Arunendra Saha Ray[†], William E. Ghann[†#], Phoebe S. Tsoi[†∓], Brian Szychowski[†], Lance T. Dockery[†], Yewon J. Pak[⁋⊥], Wenjing Li[‡], Maureen A. Kane[‡], Peter Swaan[⁋], Marie-Christine Daniel[†]*

[†]Department of Chemistry and Biochemistry, University of Maryland Baltimore County (UMBC), Baltimore, Maryland 21250, USA.

[⁋] Department of Pharmaceutical Sciences, Center for Nanobiotechnology, University of Maryland, Baltimore, 20 Penn Street, Baltimore, Maryland 21201, USA.

[‡] Mass Spectrometry Center, University of Maryland School of Pharmacy, Baltimore, Maryland 21201, USA.

ABSTRACT: The synthesis of a novel poly(propyleneimine) (PPI) dendron in gram scale as well as its use in the formation of a highly stable, dendronized gold nanoparticle (AuNP)-based drug delivery platform is described herein. The AuNP-based platform is comprised of three

complementary parts: (i) A 15 nm AuNP core (ii) A hetero-functional thioctic acid (TA)-terminated tetraethylene glycol spacer (TEG) (iii) A third generation PPI (G3-PPI) dendron with unique protonation profile and diverse end-group functionalization that allows for further derivatization. The prepared dendronized AuNPs are able to withstand several rounds of lyophilization cycles with no sign of aggregation, are stable in PBS and Hanks buffers as well as in serum, and is resistant to degradation by glutathione exchange reactions. This nanocarrier platform displays a dense coating, with >1400 dendrons/AuNP, which will enable very high payload. Furthermore, while amine-terminated AuNPs expectedly showed cytotoxicity against MCF-7 breast cancer cell line from a nanoparticle concentration of 1 nM, the mixed monolayer AuNPs (coated with 40/60 amine/carboxylate dendrons) interestingly did not exhibit any sign of toxicity at concentrations as high as 15 nM, similarly to the carboxylate-terminated AuNPs. The described dendronized AuNPs address the current practical need for a stable nanoparticle-based drug delivery platform which is scalable and easily conjugable, has long-term stability in solution and can be conveniently formulated as a powder and redispersed in desired buffer or serum.

INTRODUCTION

The current limitations of conventional drug therapy include narrow therapeutic window, systemic toxicity, lack of tissue/organ specificity and real-time- diagnosis.[1] The search for multiplexed molecules that can provide the desired triad of functions (biorecognition, specific cytotoxicity and bio-barrier evasion) is still ongoing and is an area of active research.[2] However, it is extremely difficult for a single molecule to fulfill all these requirements. One way to simultaneously address these needs is through the judicious selection of nanocarriers[3] (liposomes[4, 5], dendrimers[6, 7],

nanoparticles[8, 9,10,11,12]). Indeed, due to its size and particular structure, the use of a nanocarrier for the delivery of an existing drug can confer the drug better target specificity (thereby limiting its systemic toxicity), longer circulation time, the ability to overcome some bio-barriers and potential for real-time monitoring.[10-12]

Currently, multiple pharmaceutical companies have embarked on developing nano-based drug delivery strategies through a careful consideration of the intrinsic challenges and opportunities presented by this nascent technology.[2] The FDA has in turn approved some of the promising drug nanocarriers such as Doxil (PEG-liposome encapsulation of Doxorubicin), Onco TCS (liposomal formulation of vincristine), Abraxane (albumin bound Paclitaxel nanoparticles), Zevalin(Radio-immunoconjugate), and Zinostatin (Polymer-protein conjugate)[13]. The success of these drug nanoformulations evidences the potential of this methodology for improving cancer drug therapy.

The use of dendrimers for various drug delivery applications is also an area of intense research.[6, 7, 14, 15] Dendrimers are highly branched, globular macromolecules with multiple arms emanating from the core.[16] Their well-defined dendritic architecture allows for several advantages over the use of conventional polymers such as: (i) controlled multivalence for linkage of multiple chemical moieties,[17] (ii) very low polydispersity which in turn results in reproducible pharmacokinetic behaviors.[16] Additionally, the drug loading capacity of the dendrimers can be tuned by varying the generation number (the number of surface groups available for drug interactions doubles or triples with each increasing generation).[16] Likewise, the conjugation of the drug(s) to the dendrimer can be modulated through the nature of chemical linkage (pH sensitive[18], light sensitive[4], biodegradable[19, 20]) and many of these conjugates have shown increased solubility and/or decreased systemic toxicity. Covalent dendrimer-drug conjugates that have been

synthesized for ongoing studies have included platinum complexes (cisplatin, oxaliplatin, carboplatin), 5-fluorouracil, Ara-C, Doxorubicin, and Paclitaxel.[21] However, organic core-bearing dendrimers are limited in their sizes due to steric hindrance at higher generations and in turn in the surface area to which molecules of interest might be conjugated.

The creation of non-classical dendronized nanoparticles (NPs), also called nanoparticle-cored dendrimers (NCDs)[22, 23] can circumvent the challenges of increased steric hindrance with higher dendrimer generation by combining a relatively large inorganic gold core with the defined branched structure of organic dendrons (branched organic macromolecules with tree-like shape).[24-26] This convergent strategy synthesis also allows for increasing the number of dendritic branches from <10 (in the dendron) to hundreds or thousands (on the dendronized NP, depending on the NP core size) in a single step.[27, 28]

We have previously reported the synthesis of an amine-terminated poly(propyleneimine) PPI dendron and its use to prepare stable water-soluble dendronized AuNPs.[29] This PPI dendron displayed a protected thiol group at its focal point, the thiol function providing strong anchoring to AuNP surface and the protective group avoiding thiol interference during further dendron derivatization. While this dendron led to very stable gold nanoparticles, the use of the protective group added two steps to the preparation of the overall dendron (protection/deprotection), with the protection step presenting the poorest yield of the whole synthesis (<50%).

Herein, we report the use of thioctic acid at the focal point of the PPI dendron, as well as the synthesis of the carboxylate version of the PPI dendron, in addition to the aminated version. This brings significant advantages to both the synthesis and potential derivatization of PPI dendrons as well as the preparation of extremely stable gold nanoparticles, capped with either the

carboxylate-PPI dendron, the amine-PPI dendron, or a mixture of both. Indeed, since thioctic acid displays a cyclic disulfide, it is not expected to interfere in most common organic reactions so there is no need of protective group during the dendron preparation or conjugation: this permits to increase the overall yield of dendron synthesis and to work at gram scale. This also extends the choice for further derivatization of the PPI dendrons since there is no more restriction on derivatization conditions due to potential protective group removal, and no more limitations on the chemistry of derivatization due to potential dendritic labels cleavage during deprotection. The use of thioctic acid also adds further stability to the dendronized gold nanoparticles, since it is a bidentate ligand, as compared to a monodentate thiol group, and endows these reported dendronized AuNPs with high stability both in serum as well as after multiple freeze-drying cycles.

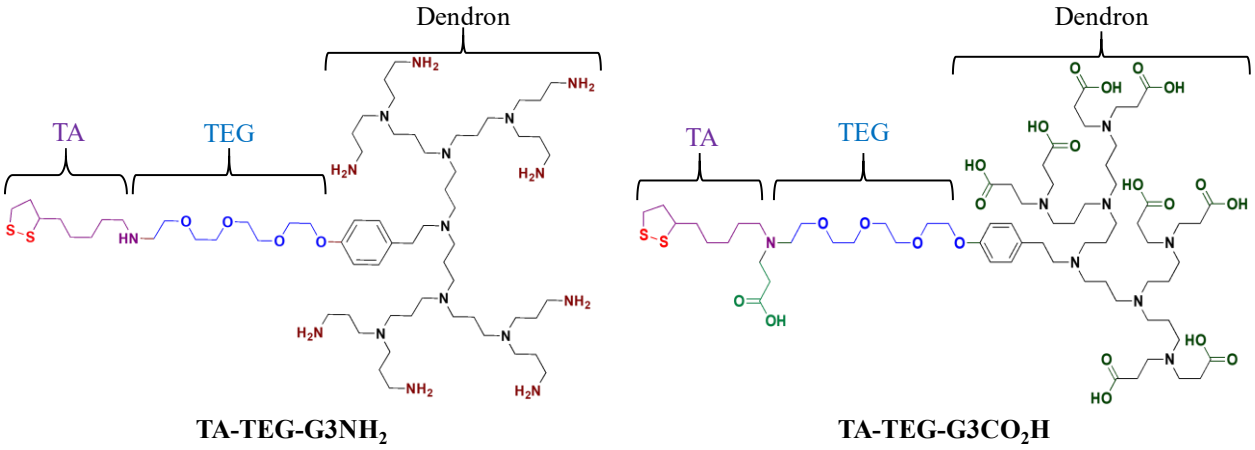

Figure 1. Set of PPI dendrons prepared: TA-TEG-G3NH$_2$ and TA-TEG-G3CO$_2$H. The sulfur atoms (red) of Thioctic Acid (TA, purple) are the anchoring points for TA-TEG-Dendron through Au-S bonds; The role of the TEG spacer (blue) is to reduce steric hindrance between arms of Generation 3 PPI dendrons (black); The terminal functional groups (brown/green) on PPI dendrons serve as points of conjugation and/or functional group interchange.

EXPERIMENTAL SECTION

Synthesis of G2-CN and G3-CN PPI Dendron: Synthesis was performed following protocols established in our lab and published in prior work.[32]

Synthesis of TA-TEG Spacer:

***TA-PFP (1)* -** Thioctic acid (10.0 g, 48.5 mmol) was dissolved in 10 mL of dichloromethane in a round-bottom flask equipped with a magnetic stir bar. While stirring, *N*,*N*′-dicyclohexylcarbodiimide (10.0 g, 48.5 mmol) was slowly added, and the mixture was stirred for 15 min. Pentafluorophenol (8.92 g, 48.5 mmol) dissolved in 10 mL of dichloromethane was then slowly added to the mixture and allowed to stir at room temperature (rt) overnight. The mixture was filtered and quenched with 80 mL of water, and the product was extracted with dichloromethane. The combined organic layers were further washed with brine, dried over sodium sulfate, filtered, and concentrated under reduced pressure. Purification by flash column chromatography (SiO_2, 9:1 hexane: ethyl acetate) yielded a yellow oil (16.2 g, 90% yield). R_f = 0.85 (9:1 hexane:ethyl acetate); ^{1}H NMR (400 MHz, $CDCl_3$) δ (ppm) 3.62-3.54 (m, 1H), 3.08-3.21 (m, 2H), 2.64-2.73 (t, 2H), 2.42-2.52 (m, 1H), 1.87-1.96 (m, 1 H), 1.64-1.86 (m, 4H), 1.46-1.64 (m, 2H). ^{19}F NMR (376 MHz, $CDCl_3$) -152.65 (d, 2F), -157.92 (t, 1F), -162.19 (m, 2F). ^{13}C NMR (100 MHz, $CDCl_3$) δ (ppm): 169.37, 142.50, 140.00, 139.90, 138.70, 56.24, 40.29, 38.61, 34.59, 33.21, 28.56, and 24.57.

***TA-TEG-OH (5)* -** TA-PFP (**1**) (4.50 g, 12.1 mmol), HO-TEG-NH_2 (**4**) (2.55 g, 13.2 mmol) and triethylamine (1.68 mL, 11.63 mmol) were dissolved in 30 mL THF and stirred overnight at room temperature. The solvent was evaporated under reduced pressure and the crude product purified

via column chromatography (10:1 EtOAc/MeOH) to obtain 3.85 g of the product as yellow oil (83 % yield); R_f = 0.58 (SiO_2, 10:1 EtOAc/MeOH). ^{1}H NMR (400 MHz, $CDCl_3$) δ (ppm) 3.76-3.38 (m, 17H), 3.20-3.06 (m, 2H), 2.44 (m, 1H), 2.18 (t, 2H), 1.89 (m, 1H), 1.74-1.57 (m, 4H), 1.51-1.35 (2H, m). HRMS (ESI) *m/z* calcd. for $C_{16}H_{32}NO_5S_2$ ($M+H^+$) 382.1716, observed 382.1714.

***TA-TEG-OTs (6)* -** To TA-TEG-OH (**5**) (8.0 g, 21 mmol) in 40 mL THF cooled to 0ºC was added a solution of sodium hydroxide (2.7 g, 67.5 mmol) dissolved in10 mL deionized water, and the solution was stirred for a few minutes. Toluene sulfonyl chloride (12.0 g, 63.0 mmol) in 30 mL THF was then added slowly using a dropping funnel. The reaction was allowed to stir at room temperature overnight. The following day, THF was removed under pressure with no additional heat on the rotary evaporator. The clear oil was then taken up in 100 mL DCM and extraction against water and brine was performed. The combined organic layers were dried over sodium sulfate, filtered and concentrated under reduced pressure. The crude product was purified *via* column chromatography (SiO_2, 95:5 EtOAc/MeOH) to yield 8.7 g of product as a bright yellow oil (78 % yield) R_f = 0.60 (SiO_2, 95:5 EtOAc/MeOH); ^{1}H NMR (400 MHz, $CDCl_3$) δ (ppm) 7.75 (d, 2H), 7.31 (d, 2H), 6.07 (s, 1H) 4.11-4.07 (m, 2H), 3.67-3.35 (m, 16H), 3.08 (m, 2H), 2.38-2.52 (m, 3H), 2.15 (t, 2H), 1.90-1.85 (m, 1H), 1.71-1.51(m, 4H) 1.51-1.33(m, 2H). ^{13}C NMR (100 MHz, $CDCl_3$) δ (ppm) 173.17, 172.91, 145.00, 132.95, 130.00, 129.96, 128.04, 70.50, 60.47, 56.52, 40.30, 39.23, 38.54, 36.39, 34.71, 28.98, 25.45. HRMS (ESI) *m/z* calcd. for $C_{23}H_{37}NNaO_7S_3$ $(M+Na)^+$ 558.1630, observed 558.1621.

Synthesis of Spacer-Dendron Conjugates:

TA-TEG-G2CN (7): G2CN was prepared according to previously published work[29]. To a solution of G2CN (1.3 g, 2.8 mmol) in 10 mL anhydrous CH_3CN, KOH (0.63 g, 11.21 mmol), K_2CO_3 (1.55 g, 11.21 mmol) and TBAB (87 mg, 0.27 mmol) was added. The reaction mixture was allowed to

stir at 45^0C for 2 h in an oil bath after which TA-TEG-OTs (**6**) (3.16 g, 5.88 mmol) was added to the reaction mixture. The final reaction mixture was set to reflux for 2 days. The reaction mixture was then dissolved in 25 mL dichloromethane and filtered to remove the solids. The organic layer was then poured in deionized water and extracted against water and brine. The combined bright orange organic layer was dried over sodium sulfate, filtered and concentrated to a clear orange oil. The orange oil was subsequently dissolved in minimum amount of dichloromethane and washed three times with ethyl acetate, Et_2O and hexane, resulting in the separation of a clear yellow oil (1.8 g, 77% yield). The supernatants collected from the washes were discarded. ^{1}H NMR (400 MHz, $CDCl_3$) δ (ppm) 7.08 (d, 2H), 6.82 (d, 2H), 4.09 (s, 2H), 3.83-3.42 (m, 16H), 3.11 (m, 2H), 2.80-2.48 (m, 31H), 2.15-1.40 (m, 11H). ^{13}C NMR (400 MHz, $CDCl_3$) 173.30, 156.98, 133.04, 129.73, 118.93, 114.47, 77.67, 77.35, 69.79, 56.48, 51.33, 49.61, 45.21, 40.26, 39.18, 36.28, 34.68, 25.43. HRMS (ESI) *m/z* calcd. for $C_{42}H_{66}N_8O_5S_2$ $[M+H]^+$ 827.4670, observed 827.4699.

TA-TEG-G2NH$_2$ (8): To a solution of **7** (1.56 g, 1.89 mmol) in anhydrous THF (40 mL) under nitrogen in a 2-neck round bottom flack was added borane dimethyl sulfide complex (14 mL, 5 equiv. per nitrile group, 20 equiv. total) using a glass syringe. The reaction mixture was stirred at room temperature (gel formation was evident on the sides of the flask after few hours). The borane dimethyl sulfide complex was added in two more additions at 4 h intervals. The resulting reaction mixture was allowed to stir overnight at room temperature under nitrogen. The next day, cold methanol was added slowly at 0^0C until no further bubbling or reaction was observed, and was then removed under reduced pressure. Fresh methanol (30 mL) was added to the residue and the solution was heated under reflux overnight. Upon cooling to room temperature, the solvent was removed under reduced pressure to yield a light yellow oil. The oily residue was taken up in 20 mL water, washed with ethyl acetate (3x10 mL) and diethyl ether (3x10 mL) and lyophilized

overnight to yield the product as a viscous yellow oil. The oil was dissolved in deionized water and further purified through a size exclusion column (LH-20) to yield a yellow oil (1.27 g, 79 % yield). Reduction of the nitriles via borane dimethyl sulfide also concurrently reduced the amide bond of the thioctic acid to an amine and the completion of this reduction was observed in the reflected mass spectra. ^{1}H NMR (400 MHz, CD_3OD) δ (ppm) 7.11 (d, 2H), 6.85 (d, 2H), 4.08 (s, 2H), 3.85-3.36 (m, 16H), 3.12 (m, 2H), 2.95-2.28 (m, 40H), 1.95-1.40 (m, 21H). ^{13}C NMR (400 MHz, $CDCl_3$) 157.30, 132.71, 129.49, 78.25, 70.44, 48.58, 47.94, 47.73, 47.52, 47.30, 39.72, 34.70, 29.52, 26.80. HRMS (ESI) *m/z* calcd for $C_{42}H_{84}N_8O_4S_2$ $[M+H]^+$ 829.6057, observed 829.6176.

TA-TEG-G3CO$_2$Me (9): To a solution of **8** (0.65g, 0.78 mmol) in 20 ml of MeOH, LiBr (110 mg, 1.25 mmol) was added and the reaction mixture was stirred for 30 min at 0 ^{0}C. Methyl acrylate (3 mL, 5 equiv. per amine, 35 mmol) was added in a dropwise manner to the cooled reaction mixture which was allowed to warm up to room temperature and further stirred for an additional 48 h. After 48 h., the excess methyl acrylate was removed from the reaction mixture via repeated stripping of the resulting oil with MeOH (4 times) followed by CH_2Cl_2 (4 times). The resulting yellow oil was taken in 20 mL CH_2Cl_2 and extracted against water, and brine. The combined organic layers were then dried over sodium sulfate and filtered to yield an clear light yellow oil (1.1 g, 88%) ^{1}H NMR (400 MHz, $CDCl_3$) δ (ppm) ($CDCl_3$) 7.03 (d, 2H) , 6.77 (d, 2H), 4.04 (s, 2H), 3.78-3.38 (m,43 H) , 3.12 (m, 2H), 2.85-2.28 (m, 62 H), 1.85-1.24 (m, 25 H), ^{13}C NMR (400 MHz, $CDCl_3$) δ (ppm) 173.27, 157.37 , 129.54, 114.36, 70.36 , 69.61,67.34, 48.13, 48.92, 31.89, 29.51, 27.13, 23.39. HRMS (ESI) *m/z* calcd for $C_{78}H_{138}N_8O_{22}S_2$ $[M+H]^+$ 1603.9445, observed 1603.9447.

TA-TEG-G3CO$_2$H (10): To the solution of **9** (0.5 g, 0.31 mmol) in 10 mL MeOH:H_20 (3:1), LiOH.H_2O (42 mg, 6 equiv. per ester branch, 16.75 mmol) was added and the reaction mixture was stirred for 24 h. After 24 h., an additional 15 mL of water was added to the reaction along with 10 mL of CH_2Cl_2. The extraction against CH_2Cl_2 (10 mL) was performed 3 times and the combined aqueous layers were further purified via dialysis (MWCO 1000) against pH7 water. The water was changed 4 times at an interval of 4-6 h. Post dialysis, the solution was lyophilized, redissolved in DI water, further purified through a size exclusion column (LH-20) in water and again lyophilized to yield an off white solid (0.38 g, 83%). Prior to MS acquisition, the product solution was desalted via a PD-10 column. MS of the sample in 0.1% acetic acid strongly showed the presence of triply charged and doubly charged species at *m/z* 493.3 [M+3H] and 739.5 [M+2H]. A low intensity signal for the $[M+H]^+$ was also observed at 1477.9 via MS. ^{1}H-NMR (400 MHz, CD_3OD) δ (ppm) 7.15 (s, 2H), 6.87 (d, 2H), 4.08 (s, 2H), 3.81-3.54 (m, 16 H), 3.11 (m, 2H), 3.12-2.43 (b, 62 H), 1.85-1.24 (b, 33 H). ^{13}C NMR (400 MHz, $CDCl_3$) 179.36, 178.55, 157.36, 129.49, 114.35, 70.42, 70.27, 67.69, 52.67, 51.58, 40.04, 38.04, 34.70, 33.83, 29.45, 28.95. ζ potential at pH 7 was - 40.6 mV. ATR-FTIR (powder); ν= 3395 O-H stretch, ν = 1725 C=O stretch, ν =1450 OH bend, ν =1085 C-O bending; HRMS (ESI) *m/z* calcd. for $C_{69}H_{120}N_8O_{22}S_2$: 1476.8 Da; observed mass: 1476.9 Da (both are monoisotopic masses).

TA-TEG-G3CN (11): G3CN was prepared as previously reported in the literature. G3CN (0.96 g, 1.6 mmol) was dissolved in 10 mL of anhydrous acetonitrile. To the G3CN dendron, 4 equiv. of KOH (0.36 g, 6.4 mmol) and K_2CO_3 (0.88 g, 6.4 mmol) was added along with 63 mg (0.19 mmol). Tetrabutyl ammonium bromide (TBAB) was added and allowed to stir for 1 h. in an oil bath at 50^{0}C. To this mixture, TA-TEG-OTs (**6**) (1.8 g, 4.2 mmol) dissolved in 15 mL CH_3CN was added and set to reflux for 2 days. After 2 days, the reaction mixture was filtered to remove any solids

and the organic mixture was removed under pressure to yield a viscous orange oil. The orange oil was dissolved in 20 mL of CH_2Cl_2 and extracted twice against water and once against brine. The combined organic layers were dried over sodium sulfate, filtered and concentrated to a clear orange oil which was dissolved in a minimum of CH_2Cl_2 and washed 4 times with hexane and diethyl ether to produce a clear orange oil. The supernatant from the washes were discarded. (1.48 g, 74 % yield). ^{1}H NMR (400 MHz, $CDCl_3$) δ (ppm) 7.05 (d, 2H), 6.78 (d, 2H), 4.05 (s, 2H), 3.78-3.35 (m, 16H), 3.07 (m, 2H), 2.78-2.43 (m, 62H), 2-1.1 (m, 20). ^{13}C NMR (400 MHz, $CDCl_3$) 129.70, 114.60, 70.61, 69.87, 67.50, 49.67, 37.69, 34.24, 29.12. HRMS (ESI) *m/z* calcd. for $C_{66}H_{106}N_{16}O_5S_2$ $[M+H]^+$ 1267.7924, observed 1267.8062.

TA-TEG-G3NH$_2$ (12): To a solution of **11** (1.5 g, 1.18 mmol) in anhydrous THF in a 2-neck round bottom flask under nitrogen, borane dimethyl sulfide complex (4.5 mL, 5 equiv. per nitrile branch, 47 mmol) was slowly added using a syringe. The reaction mixture was allowed to stir (gel formation was evident after few hours). Two further additions of borane dimethyl sulfide complex were performed at 3-4 h. intervals. The reaction mixture was allowed to stir overnight at room temperature under inert conditions. The next day, methanol was added slowly at 0^0C until no further bubbling or reaction was observed. The solvent was then removed under reduced pressure. Fresh methanol (30 mL) was added to the reaction and was heated under reflux overnight. Upon cooling to room temperature, the solvent was removed under reduced pressure to yield a light yellow oil. The oily residue was taken up in 20 mL water and extracted against ethyl acetate (2x10 mL) and diethyl ether (2x10 mL). The combined aqueous layers were lyophilized overnight to yield the product as a viscous clear off white oil. The oil was dissolved in deionized water and further purified through size exclusion column (LH-20) followed by dialysis (MWCO 1000). The dialysis water was changed 3 times at 4-6 h. intervals. Post dialysis, the aqueous solution was

lyophilized to yield a very light yellow powder (1.08 g, 71 % yield). ^{1}H NMR (400 MHz, $CDCl_3$) δ (ppm) 7.25 (d, 2H), 6.92 (d, 2H), 4.09 (s, 2H), 3.78-3.35 (m, 16H), 3.07 (m, 2H), 3.28-2.43 (m, 78H), 2.26-1.16 (m, 38H).^{13}C NMR (400 MHz, H_2O) 162.88, 130.45, 114.99, 72.82, 70.42, 70.10, 60.67, 40.62, 39.78, 39.78, 39.37, 31.31, 26.7; ATR-FTIR (powder): ν = 3357, 3262 primary amine N-H stretch, ν =1654 N-H bending. ζ potential at pH 5 was +31.2 mV. HRMS (ESI) *m/z* calcd. for $C_{66}H_{140}N_{16}O_4S_2$ $[M+H]^+$ 1286.0685, observed: $[M+H]^+$ 1286.0869.

Synthesis and studies of gold nanoparticles:

Synthesis of Citrate AuNPs: All glassware and stir bars were cleaned with aqua regia and rinsed a minimum of 10 times with ultrapure water. A gold salt stock solution was prepared by dissolving $HAuCl_4$ (0.1 g in 10 mL) in ultrapure water to yield a 28.31 mM stock solution. Sodium citrate stock solution was prepared by dissolving 1 g sodium citrate in 20 mL water (0.17 M). 2.65 mL of gold salt stock solution was added to 247.5 mL ultrapure water in a two-neck round bottom flask equipped with a condenser and a stir bar, and heated to reflux in an oil bath. Once the solution was refluxing, 4.41 mL of sodium citrate stock solution was added to the reaction mixture and stirred vigorously under reflux. The gold salt to citrate molar ratio used was 1:10. After 20 minutes, the heat was stopped and the solution was kept stirring while cooling down to room temperature. UV-Vis and DLS spectra were recorded to characterize the AuNPs. The DLS size by number was 21.4 nm.

AuNP Ligand Exchange Reactions: 200 mL of citrate AuNPs (2.46 nM) was centrifuged at 10,000 g, for 60 min at 6^0C to remove some of the excess citrate. The clear supernatant was then removed very carefully and discarded to yield a dark red pellet which was subsequently dissolved in 30 mL ultrapure water. The absorbance of the citrate AuNP solution at 450 nm was used to

calculate the AuNP concentration.[30] After the calculation of citrate-stabilized AuNP concentration, the number of ligand required for complete coverage of the AuNP surface was calculated and a minimum of 40X the molar amount was used for ligand exchange using both synthesized dendrons (Figure S24).

Singly dendronized AuNPs - The amine-terminated dendron (**TA-TEG-G3NH$_2$**) was dissolved in 2 mL ultrapure water (pH 5.5) and the carboxylate-terminated dendron (**TA-TEG-G3CO$_2$H**) was dissolved in ultrapure water adjusted to pH 9 using $NaHCO_3$ to ensure complete solubility of respective dendrons. Prior to the addition of the dendron solution to a rapidly stirring solution of AuNPs, the samples were filtered through a 0.22 μm syringe filter. Upon addition of the dendron solution, the bright reddish AuNP solution turned to a slightly darker red. The solutions were allowed to stir under ambient condition for 20-22 h. prior to purification and removal of excess ligands via centrifugation at 10,000 g, 45 min at 6^0C (2-3 rounds).

Mixed-monolayer dendronized AuNPs – First, two solutions of amine-terminated dendron (TA-TEG-G3NH$_2$) and carboxylate-terminated dendron (TA-TEG-G3CO$_2$H), respectively, were prepared separately by dissolving each in 1 mL ultrapure water adjusted to pH 7 using $NaHCO_3$. Then the appropriate volumes from each solution were combined to obtain a mixture composed of 60% TA-TEG-G3CO$_2$H and 40% TA-TEG-G3NH$_2$ (molar ratio). This mixture was filtered through a 0.22 μm syringe filter and added to a solution of AuNPs that had been previously centrifuged and redispersed in ultrapure water, as explained for the singly dendronized AuNPs. The AuNP solution turned to a very slightly darker red (if the solution turns purplish, then add a drop or two of 1M HCl). The AuNP solution was allowed to stir under ambient condition for 20-22 h. prior to purification and removal of excess ligands via centrifugation at 10,000g, 45 min at 6^0C (2-3 rounds).

TGA: The dendronized AuNPs were purified extensively prior to the dendron quantification studies via thermogravimetric analysis. The crude dendronized AuNPs were centrifuged 2 times for 75 min at 12,000g at 5^0C. After each centrifuge cycle, the colorless supernatant was carefully removed and the remaining dark red pellet was re-suspended in ultrapure water. Post centrifugation, the AuNP solution was dialyzed (MWCO: 12,000 Da) three times against ultrapure water. The resulting AuNP solution was centrifuged a third time at 10,000g, 5^0C for 60 min. The supernatant was discarded and the reddish black pellet was suspended in 15 mL ultrapure water and transferred to a lyophilization chamber. The AuNP samples were lyophilized for 3 days to ensure complete removal of trace amounts of water. The resulting black colored AuNP powders were used for TGA analysis. TGA analysis was run in duplicates for both samples with sample weights ranging from 1.3 mg to 1.6 mg.

Lyophilization Studies: The dendronized AuNPs from AuNP ligand exchange reaction were purified according to the procedure outlined in the TGA sample preparation prior to the dialysis stage. Post centrifugation of AuNP, the supernatant was discarded and the reddish black pellet was suspended in 20 mL ultrapure water. From the 20 mL batch, a 5 mL aliquot was taken for running UV-Vis and DLS data collection. After the acquisition of UV-Vis and DLS spectra, the sample was lyophilized for 2 days. The resulting powder was dissolved in exactly the same volume of 5 mL water and was lyophilized. The prior steps of dissolution of AuNPs, data acquisition and lyophilization was performed for two additional rounds on the same sample, yielding 3 data points per dendronized AuNP. Care was taken to maintain the same AuNP concentration (2.6 nM) through the three lyophilization rounds.

Stability Studies: The lyophilized AuNP powders derived as per the procedure in prior steps were dissolved in 2 mL neat solution of buffers and salts with the exception of the serum solution. The

concentration for AuNP used for the stability studies were 1.8 nM. The sample preparation for the study of stability in serum was performed by first dissolving the AuNPs in 250 μL of ultrapure water to which 1.75 mL human serum was added. All DLS data for stability studies were acquired at 37^0C with an incubation time of 3 minutes. UV-Vis data of samples were acquired immediately following DLS data acquisition. The samples were maintained through the entire 7 day period in a water bath maintained at 37^0C.

Evaluation of Cytotoxic Profile of Dendronized AuNPs: MCF-7 cells were grown in a 250 mL cell culture flask using high-glucose DMEM serum at 37^0C in a humidified atmosphere of 5% CO_2. Cell line was maintained by passaging when cells exhibited 80% confluence. In order to assess the cytotoxic profile of AuNP-G3NH_2, AuNP-G3CO_2H and AuNP-G3CO_2H/NH_2 (60/40), the respective purified nanoparticle formulations were lyophilized overnight to yield a black powder. The AuNP powders were suspended in DMEM media via mixing with a sterile 1 mL pipette to generate 15.6 nM initial concentrations. All cytotoxic tests and re-dispersions were carried out within a BSL-2 laminar flow hood. MCF-7 cells were seeded and dosed according to the protocol outlined above. Cell viability was determined through the equation: Cell viability (%) = (Sample absorbance at 460 nm - background absorbance at 600 nm)/ (Absorbance of negative control at 460 nm - background absorbance at 600 nm).

RESULTS AND DISCUSSION

Scheme 1. Synthesis of TA-TEG-OTs spacer from commercially available thioctic acid (TA) and tetraethylene glycol (HO-TEG-OH) precursors.

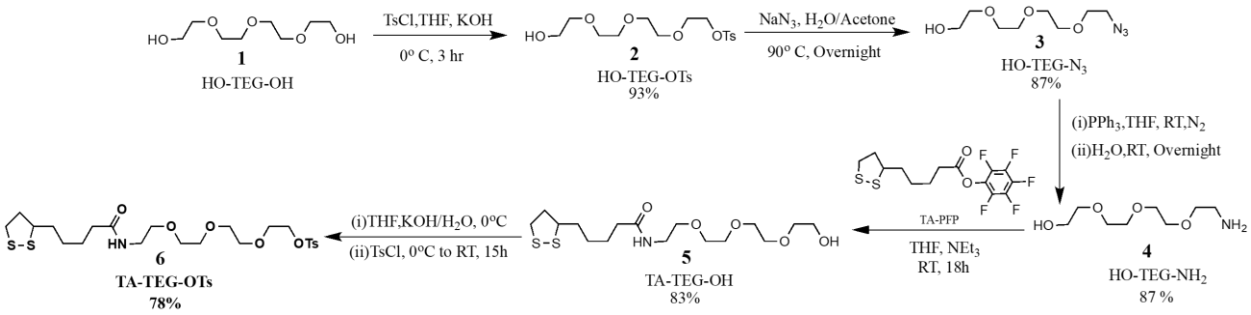

Design and Synthesis of TA-TEG-PPI Dendrons

In order to ensure the production of a scalable, easily amenable to multifunctionalization, and very stable water-soluble dendronized nanoparticle system that can carry very large payloads, we devised a dendron platform composed of three essential components (Figure 1): (1) a PPI dendritic system, which can display either carboxylate or amine termini for convenient further derivatization with desired payload, and whose commercial precursors are affordable, and readily available from commercial sources (2) a tetraethylene glycol (TEG) spacer, that allows for maximum coverage of the nanoparticle surface by reducing steric hindrance between dendritic branches, and (3) a thioctic acid (TA) group at the end of the TEG spacer, which imparts very strong AuNP anchoring ability to the dendron.[31]

The use of TA as anchoring point of the dendron to the AuNPs brings two major advantages over the use of a thiol group: (i) TA provides a stronger attachment to gold surfaces due to the bidentate nature of its terminal cyclic disulfide group,[31-33] and (ii) it eliminates the need for a protective

group, thus removing 2 steps (protection/deprotection) from the synthetic route. This absence of protective group alleviates any concern in the choice of reaction conditions during further derivatization of the dendritic branches.

The PPI dendron platform was obtained by first preparing the TA-TEG spacer and the PPI dendron and then coupling them together. This synthetic approach allowed us to prepare the TA-TEG spacer (Scheme 1) at multigram scale (with each step affording over 85% yield) and the final dendron platform in gram amounts (Schemes 2 and 3).

Scheme 2. Synthesis scheme for TA-TEG-G3NH$_2$

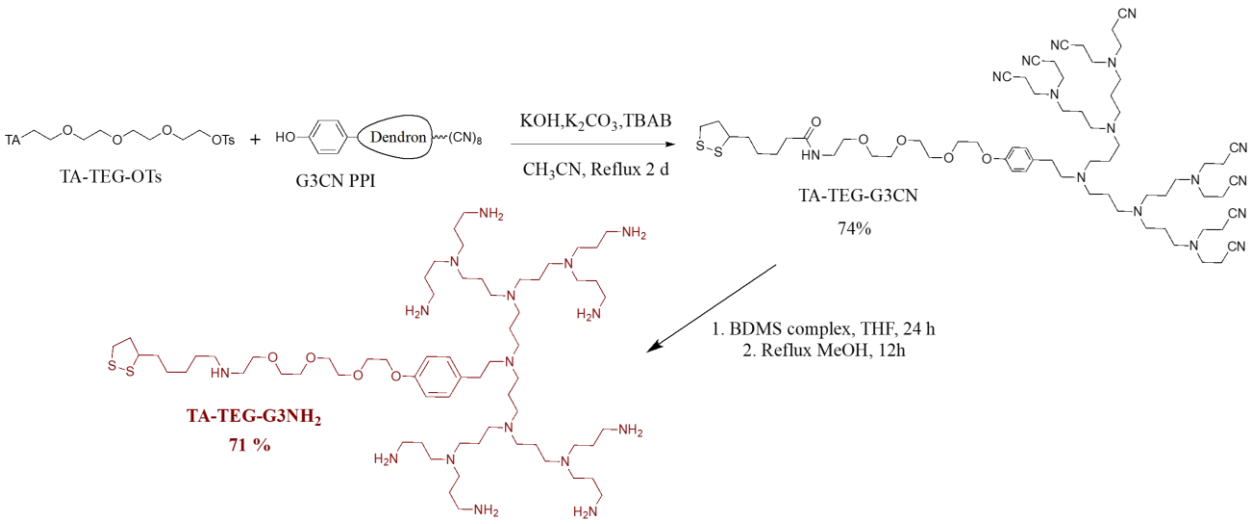

Scheme 3. Synthesis Scheme of TA-TEG-G3CO_2H

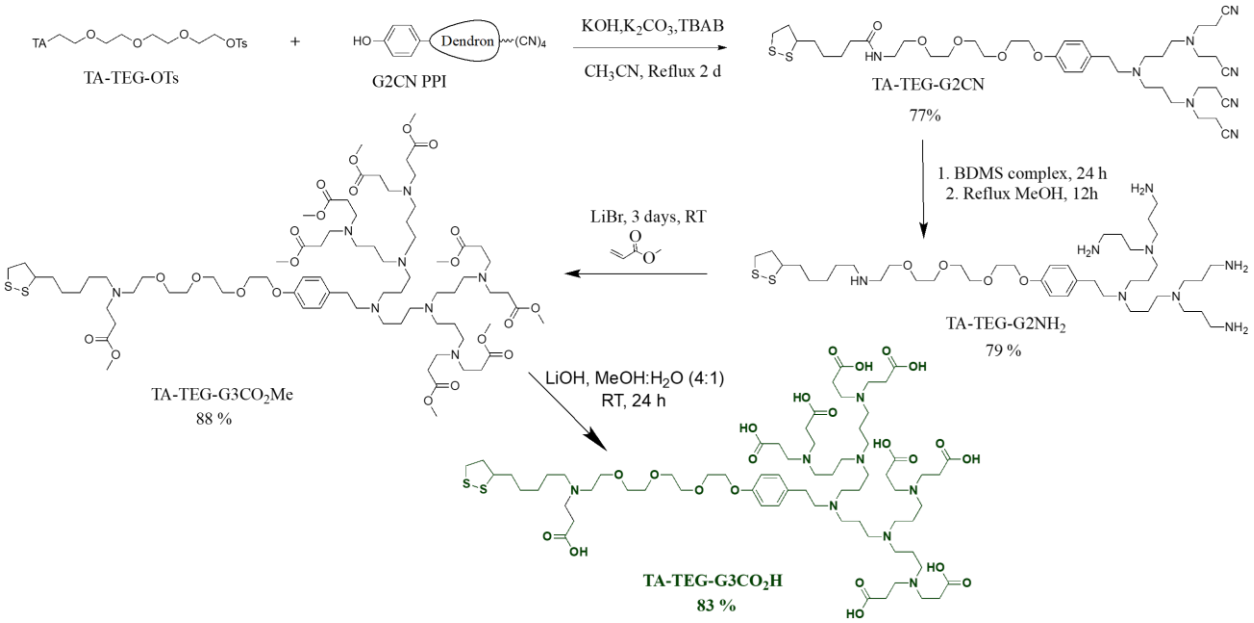

Two different synthetic routes were used to prepare the amine-terminated PPI dendron and the carboxylate-terminated PPI dendron due to the nature of the chemistry involved in the formation of classical PPI dendron. Indeed, the usual synthetic scheme for the growth of PPI dendrimers or dendrons involves a repetitive sequence of hetero Michael addition using acrylonitrile followed by reduction of the nitrile groups to primary amines.[34] This sequence of steps directly leads to the amine-terminated PPI dendron.

Consequently, for the formation of TA-TEG-G3NH_2, we first prepared the third generation nitrile-terminated dendron (G3CN) with a phenol group as focal point, then coupled it to the spacer (TA-TEG-OTs) through nucleophilic substitution at the phenol group, and finally reduced the dendritic nitrile groups to amines using borane dimethyl sulfide. Coupling G3CN instead of G3NH_2 to the spacer avoids any competition of the amine termini with the phenol group, which could result in attachment of the spacer not only to the focal point but also to the dendritic branches. It is

interesting to note that the last step, reducing TA-TEG-G3CN into TA-TEG-G3NH_2 concurrently reduces the amide bond in the spacer, between TA and TEG, which is evidenced by the mass spectrometry data (Figure S5): indeed, the observed mass on the MS data lacks 14 Daltons (16 Daltons less due to the loss of the oxygen of the amide group and 2 Daltons more from the 2 protons of the reduced amide to secondary amine) compared to the calculated mass for TA-TEG-G3NH_2 containing the amide bond. Other characterization data were collected for TA-TEG-G3NH_2, and are displayed in Figure 2. The ^{1}H NMR spectrum in D_2O (Figure 2A) shows the peaks from the protons of the dendritic branches spanning from 2 ppm to about 3.3 ppm. The protons from the TEG part give peaks between 3.4 and 4.1 ppm and the thioctic acid portion gives rise to peaks mostly between 1 and 2 ppm, but also hidden within the dendritic peaks, between 2 and 3.4 ppm. The aromatic focal point of the dendron is represented by the two peaks at 6.9 and 7.2 ppm. The presence of the terminal primary amine groups is clearly illustrated by the FTIR bands at 3357-3262 cm^{-1} (primary amine N-H stretch) and 1654 cm^{-1} (N-H bending). Finally, the positive zeta potential (30.1 mV) of TA-TEG-G3NH_2 at pH 7 also reflects the presence of the primary amine groups, which are expected to be protonated at this pH.

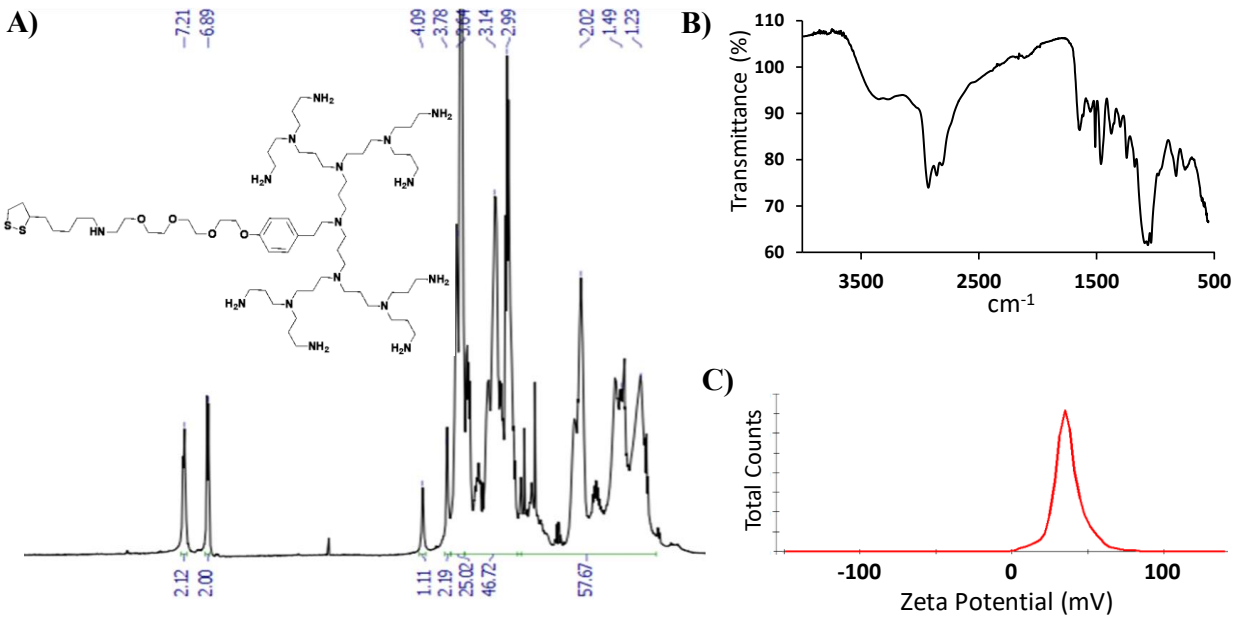

Figure 2. Characterization of TA-TEG-G3NH_2 dendron. A) ^{1}H NMR of TA-TEG-G3NH_2 dendron in D_2O with water suppression. B) ATR-FTIR of TA-TEG-G3NH_2 powder ν = 3357, 3262 primary amine N-H stretch, ν = 2928 C-H unsaturated carbon, ν =1654 N-H bending, ν = 1467 C-H bend. C) Zeta Potential (ζ) of TA-TEG-G3NH_2 at pH 7.

For the preparation of TA-TEG-G3CO_2H, the last Michael addition needs to involve methyl acrylate in order to lead to carboxylate termini after hydrolysis of the esters. Since on one hand coupling G3CO_2H to the spacer would not be efficient due to solubility issues as well as potential side reactions, and on the other hand the dendron-spacer coupling reaction requires the use of bases that would hydrolyze G3CO_2Me during its coupling to the spacer, we decided to couple the spacer to the second generation nitrile-terminated dendron (G2CN). After obtaining TA-TEG-G2CN, we then continued the growth of the dendron through Michael addition using methyl acrylate and obtained TA-TEG-G3CO_2H by hydrolysis using lithium hydroxide.[35] Interestingly, following this synthetic path results in the addition of a ninth branch to the final TA-TEG-G3CO_2H. Indeed, in order to keep growing the dendritic branches after coupling to the spacer, TA-TEG-G2CN is

reduced to TA-TEG-G2NH_2: during this reduction, the amide bond between TA and TEG also gets reduced into a secondary amine,[36] which results in TA-TEG-G2NH_2 displaying nine amines (8 dendritic primary amines and one secondary amine from the spacer). Consequently, the use of an excess (required for the dendritic branches) of methyl acrylate during the following reaction leads to nine –$CH_2CH_2CO_2Me$ branches in TA-TEG-G3CO_2Me. The final hydrolysis results in TA-TEG-G3CO_2H, which contains nine $CH_2CH_2CO_2H$ branches, as evidenced by ^1H NMR integration as well as mass spectrometry data. The MS data displays two prominent peaks: one corresponding to the doubly-protonated species (M+2H), and one for the triply-protonated species (M+3H) (Figure S7). Other characterization data were collected for TA-TEG-G3CO_2H, and are displayed in Figure 3. The ^1H-NMR spectrum in D_2O (Figure 3A) shows the peaks from the protons of the dendritic branches spanning from 1.6 ppm to about 2.95 ppm. The protons from the TEG part gives peaks between 3.5 and 4.1 ppm and the thioctic acid portion gives rise to a peak at around 1.35 ppm, but has also other peaks hidden within the dendritic peaks, between 1.7 and 3.4 ppm. The aromatic focal point of the dendron is represented by the two peaks at 6.8 and 7.1 ppm. The presence of the terminal carboxylate groups is clearly illustrated by the FTIR bands at 3395 cm^{-1} (O-H stretch), 1725 cm^{-1} (C=O stretch) and 1450 cm^{-1} (OH bend). Finally, the negative zeta potential (- 40.6 mV) of TA-TEG- G3CO_2H at pH 7 also reflects the presence of the carboxylate groups, which are expected to be deprotonated at this pH.

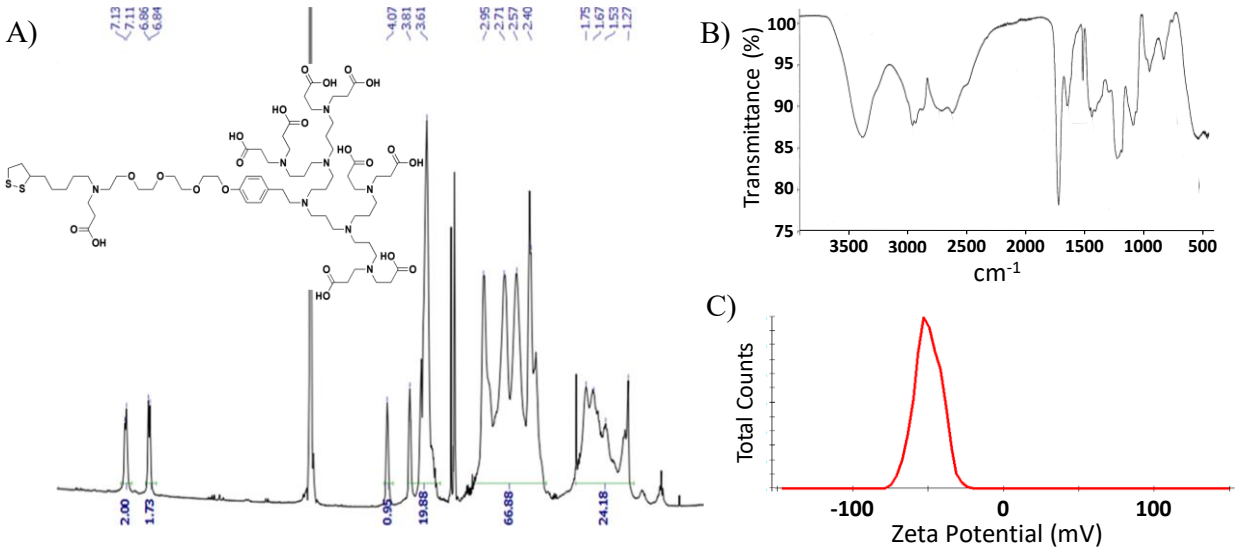

Figure 3. Characterization of TA-TEG-G3CO_2H dendron. A) ^{1}H NMR of TA-TEG-G3CO_2H dendron in D_20 with water suppression. B) ATR-FTIR of TA-TEG-G3CO_2H powder; ν= 3395 O-H stretch, ν = 2969 unsaturated C-H stretch, ν = 1725 C=O stretch, ν =1450 OH bend, ν =1085 C-O bending. C) Zeta Potential (ζ) of TA-TEG-G3CO_2H at pH 7.

Dendronized AuNPs Syntheses and Characterization:

a) Synthesis

To ensure complete exchange of the citrate molecules with TA-TEG-dendrons on the AuNPs, a minimum of 40 times excess of the TA-TEG-dendron required for total surface coverage was used for each ligand exchange reaction (Figure S24). In addition, we have experimentally determined that the polydispersity indexes (PDI) of dendronized nanoparticles were not consistent between batches when less than 40 times equivalence of dendrons were used. Furthermore, removal of excess citrate prior to ligand exchange led to lower variability in resulting AuNPs polydispersity after ligand exchange across different dendron platforms. It is noteworthy to point out that the

presence of excess citrate did not affect the PDI of the AuNP-G3CO_2H as much as it did for the AuNP-G3NH_2. We hypothesize that, during formation of AuNP-G3NH_2, facile and quick ligand exchange on the Au surface was hindered due to electrostatic attraction between the negatively charged excess citrate and positively charged amine dendrons. On the other hand, steric repulsion between the negatively charged dendron-carboxylate and citrate prevented any interference of the excess citrate in the ligand exchange on the AuNPs. Similar findings have been reported on the instability of cationic AuNPs due to the presence of citrate.[37] Overall, the removal of excess citrate prior to ligand exchange circumnavigated the discussed difficulties and led to uniformity in the preparation of all batches of dendronized AuNPs.

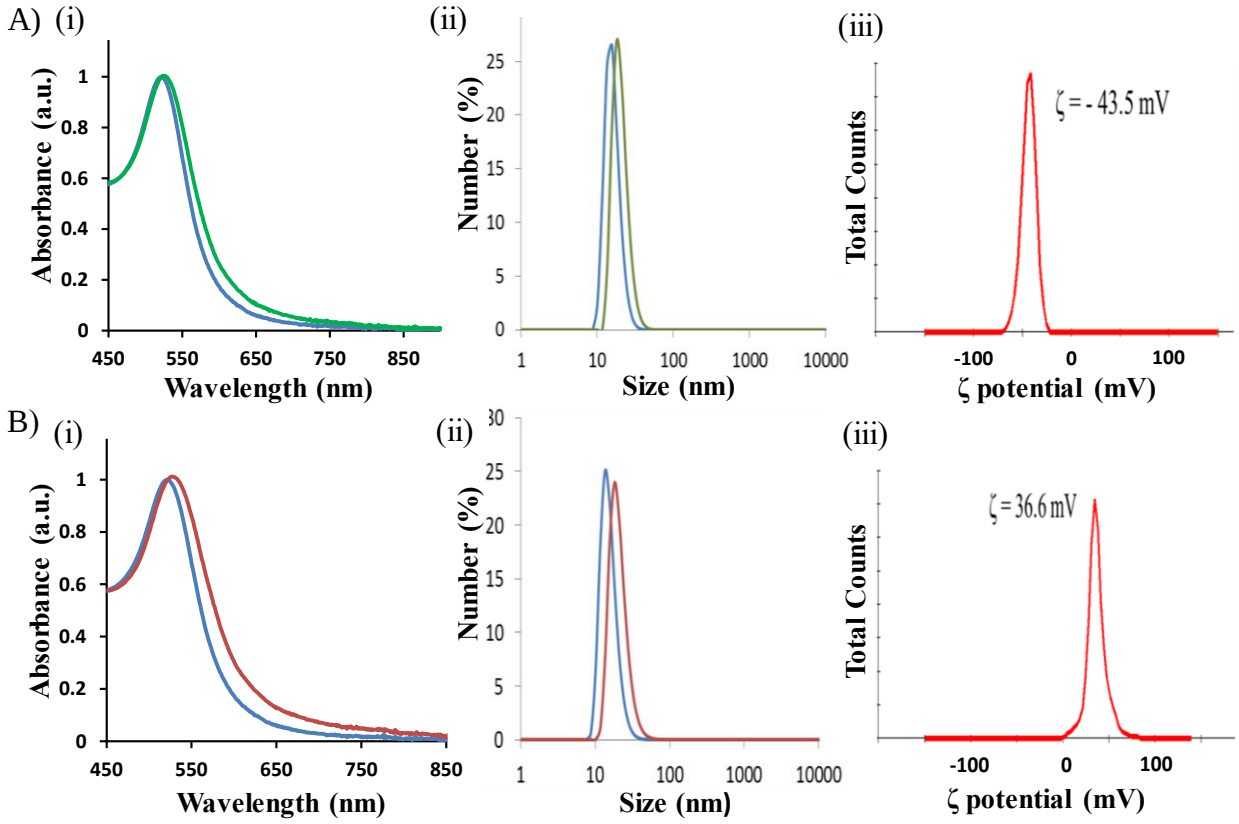

Figure 4. A) Characterization of AuNP-G3CO_2H: (i) UV-Vis spectra comparison of citrate AuNPs (blue) vs AuNP-G3CO_2H (green), Ligand exchange causes an SPR red-shift of 4 nm; (ii) DLS

comparison of citrate AuNPs (blue) vs AuNP-G3CO_2H (green) (16.1 nm, PDI 0.05 to 20.4 nm, PDI 0.09); (iii) Zeta Potential (ζ) of AuNP-G3CO_2H at pH 5.5. B) Characterization of AuNP-G3NH_2: (i) UV-Vis spectra comparison of citrate AuNPs vs AuNP-G3NH_2 (SPR red-shift of 3 nm); (ii) DLS comparison of citrate AuNPs vs AuNP-G3NH_2 (15.6 nm, PDI 0.06 to 19.9 nm, PDI 0.17); (iii) Zeta Potential (ζ) of AuNP-G3NH_2 at pH 5.5.

b) Characterization

The purified dendronized AuNPs showed excellent stability in ultrapure water (pH 5.5) (stable > 6 months) as a consequence of high steric stability and electrostatic repulsion between highly charged particles as evidenced by zeta potential characterization (Figure 4): in pure water (pH 5.5) the zeta potentials of AuNP-G3CO_2H and AuNP-G3NH_2 are – 43.5 mV and 36.6 mV, respectively. The size of the AuNPs in solution increased from 16.1 nm (DLS by number) for AuNP-citrate to 20.4 nm for AuNP-G3CO_2H and from 15.6 nm to 19.9 nm for AuNP-G3NH_2, which corresponds to an overall increase of 4.3 nm in both cases. This indicates that the hydrodynamic size of dendron coating is 2.15 nm. This corresponds well to the hydrodynamic diameter measured by DLS for the dendron alone (2.3 nm by number).

Dendronized AuNPs with mixed-coating (AuNP-G3CO_2H/NH_2, 50/50 molar ratio of TA-TEG-G3CO_2H and TA-TEG-G3NH_2) were also prepared and characterized (Figure 5). The ligand exchange of citrate by the mixture of dendrons led to a surface plasmon resonance (SPR) peak shift of 13 nm (521 nm to 534 nm), which is larger than for the singly dendronized AuNPs. Also, the hydrodynamic diameter increased from 17.9 nm (DLS by number) for AuNP-citrate to 41.6 nm for AuNP-G3CO_2H/NH_2, which represents an overall size increase of 23.7 nm and is equivalent to a dendritic coating thickness of 11.8 nm. Both the absorption and DLS data seem to

indicate the formation of a dendron multilayer around the AuNPs with mixed-coating, as opposed to the monolayers formed around singly dendronized AuNPs.

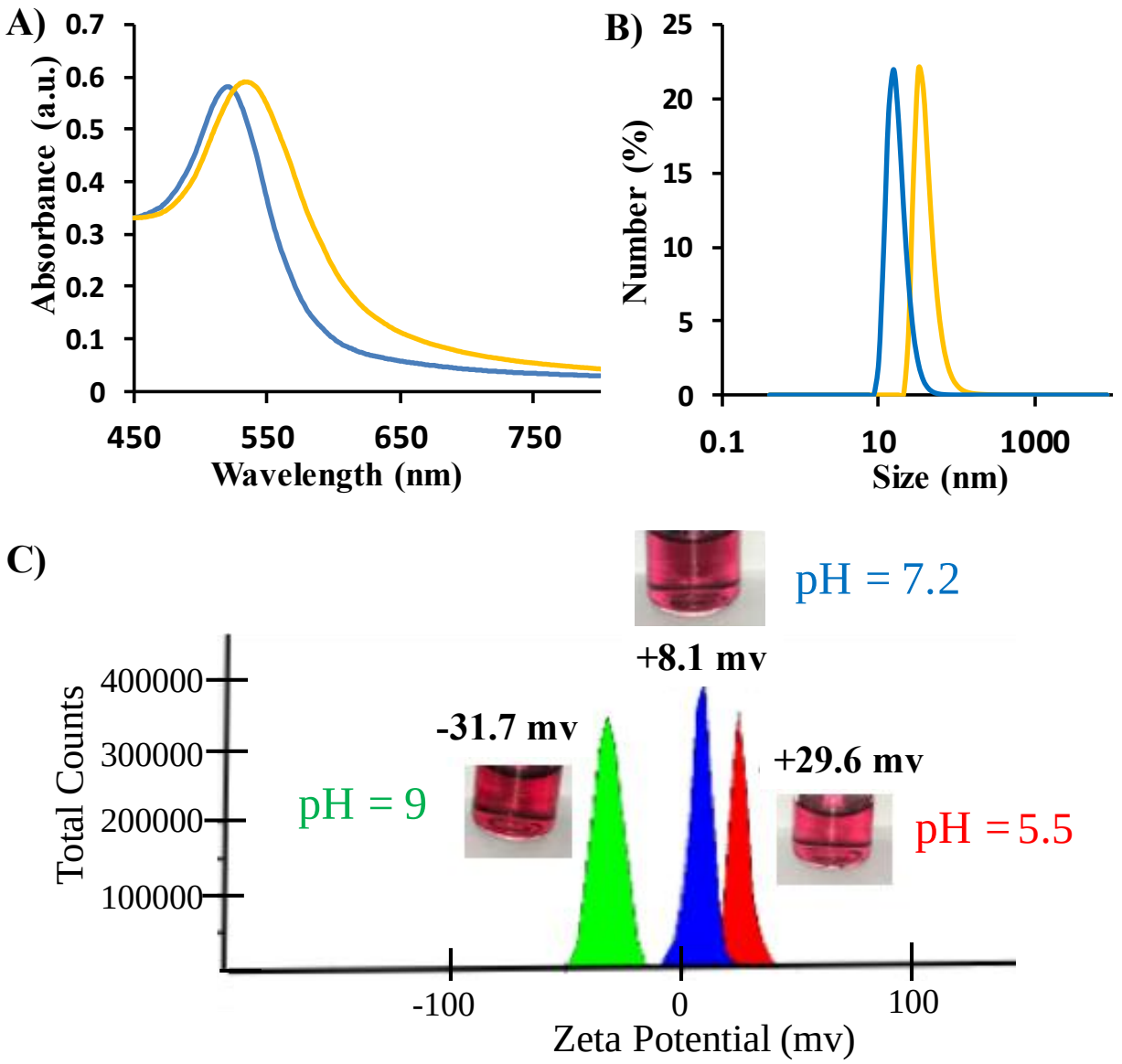

Figure 5. Characterization of mixed-coated AuNP-G3CO_2H/NH_2 (50/50): A) UV-Vis spectra comparison of citrate AuNPs (blue) vs AuNP-G3CO_2H/NH_2 (orange); B) DLS comparison of citrate AuNPs (blue) vs AuNP-G3CO_2H/NH_2 (orange); C) Zeta potential analysis at pH10 (green), pH7 (blue) and pH5 (red) - Insets correspond to NP colors at each pH value.

We have also tested AuNP-G3CO_2H/NH_2 (50/50) at different pHs (Figure 5C), and as expected, the AuNPs show an overall negative charge (- 32 mV) at pH10, due to the carboxylate groups, a positive charge (30 mV) at pH5 due to the ammonium groups, and a nearly neutral charge (8 mV) at pH7, likely coming from equal partial deprotonation and protonation of carboxylate and amine groups, respectively. This evolution of charge reflects well the dendrons composition on these mixed-monolayer dendronized AuNPs.

TEM images (Figure 6C) obtained by staining AuNPs with 2% uranyl acetate allowed for visualization of the dendron corona around the nanoparticles, with an average thickness of 1.6 nm. The apparent reduction in dendron thickness calculated from TEM measurements compared to the DLS data (2.15 nm) can be explained by the difference in sample preparation: the DLS measurements are done in solution and at atmospheric pressure, thus the nanoparticles coating corresponds to fully hydrated dendrons; but the TEM measurements are done on dry samples and under vacuum, thus the nanoparticles coating corresponds to contracted dendrons. Further STEM images (Figures S9, S10) of concentrated dendronized AuNPs also showed spherical shapes with no apparent aggregation upon visualization.

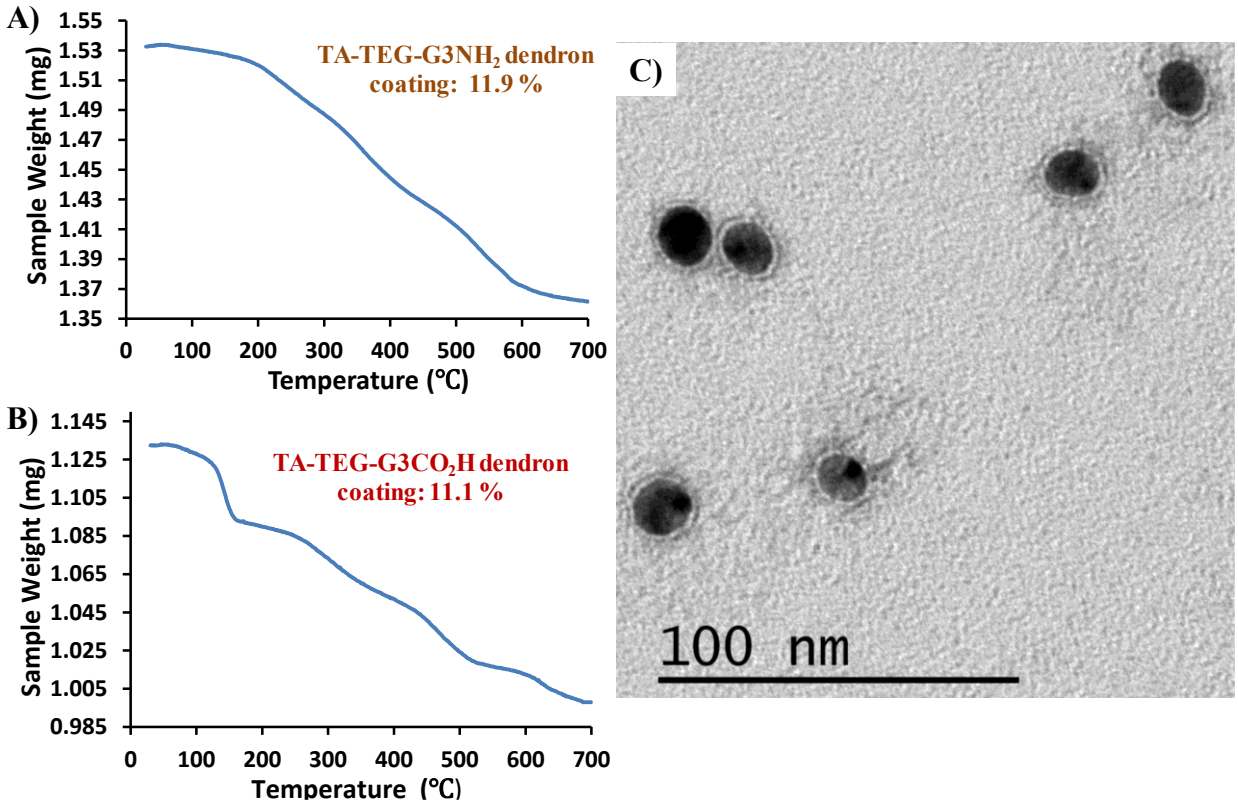

Figure 6. Surface coating of dendronized AuNPs. A) TGA analysis of dendron coating on AuNP-G3CO_2H. B) TGA analysis of dendron coating of AuNP-G3NH_2 NPs. C) TEM image of AuNP-G3CO_2H stained with 2% uranyl acetate for visualization of dendron corona: average thickness of 1.6 nm.

In order to quantify the extent of surface coating, TGA analyses were performed. The TGA data indicated that the surface coating of dendrons represents 11.8 and 11.2 % of the AuNPs masses, for AuNP-G3NH_2 and AuNP-G3CO_2H respectively (Figure 6A, 6B), which equates to around 1350 and 1450 dendrons/NP, respectively, calculated via a formula accounting for the core of the nanoparticle and molecular weight of the dendron (Figure S25). The lower number of dendrons on AuNP-G3CO_2H can be explained by the presence of 9 arms in TA-TEG-G3CO_2H compared to the 8 arms in TA-TEG-G3NH_2 (see discussion above). The added lateral steric hindrance from the

9th arm leads to a slightly lower dendron packing on the nanoparticle surface. However, this slight reduction did not contribute to a lack of nanoparticle stability, as showcased in various stability studies (vide infra). The surface density of the dendrons on the AuNPs was calculated to be around 2.3 dendron/nm^2 for AuNP-G3CO_2H and 2.5 dendron/nm^2 for AuNP-G3NH_2, which represents a high ligand density but is still realistic as it corroborates well with other observed surface densities.[38-41]

We also performed some pH studies, and noticed that the zeta potential of AuNP-G3NH_2 increases from 36.1 mV at pH 5.5 to 54.3 mV at pH 3 (Figure S10). This increase in positive charges is most likely coming from the protonation of the tertiary amines of the dendrons, which we have reported earlier.[24] This observation showcases the potential of these dendronized nanoparticles to act as proton sponges at the lysosomal pH of 4.5.

Although other dendrons also using TA as anchoring point,[25] or also presenting carboxylate or amine termini[42] have been reported in the literature for the preparation of dendronized nanoparticles, our TA-TEG-G3PPI dendrons bring two main advantages. The first difference is the addition of the TEG linker between the thioctic acid group and the PPI dendron itself: this counter-balances the steric hindrance of the eight dendritic branches of each dendron around the gold core, thus allowing very high packing and dense coating on the AuNPs. The other benefit is our preparation of *a pair of cationic and anionic PPI dendrons* that differ only in the nature of their termini (amine or carboxylate): which allowed us to combine them and prepare the first zwitterionic dendronized AuNPs.

Stability Studies

a) Lyophilization

In order to test their ease of handling, we investigated the stability of our dendronized nanoparticles against repeated lyophilization cycles. As outlined in Figure 7, both AuNP-G3CO_2H and AuNP-G3NH_2, as well as remained stable even after three rounds of freeze-dry/reconstitution cycles, regardless of the nature of their end group functionality: their hydrodynamic diameter showed negligible change after each round. Similar stability was observed for AuNP-G3CO_2H/NH_2 (Figure S26a). We can also note that all of the lyophilized nanoparticles readily redissolved in water, without leaving any precipitate residue. This very high stability is conferred to the nanoparticles by the bidentate nature of the thioctic acid moiety at the end of the dendritic focal point,[33] but also by the high packing density of TA-TEG-dendrons and the steric repulsion between charged dendronized nanoparticles. So far, only very few studies have reported other thiol-protected AuNPs to withstand several rounds of freeze-drying: one featuring cationic ligands,[42] one using anionic ligands,[43] and one with zwitterionic ligands.[44] Our present work shows that both TA-TEG-G3CO_2H and AuNP-G3NH_2 lead to very stable anionic and cationic AuNPs, respectively, and also offers the possibility of creating zwitterionic AuNPs starting from non-zwitterionic ligands. These results provide a more versatile solution to the impracticality of storage and long term handling of nanoparticles in solution. Indeed, since these dendronized nanoparticles are resistant to multiple freeze-dry cycles, they can be stored as powders and reformulated directly into the desired medium (buffers, serum, etc.) right before use. But they also have the additional advantage of presenting two alternatives for further payload conjugation, through either the carboxylate groups or the primary amine groups.

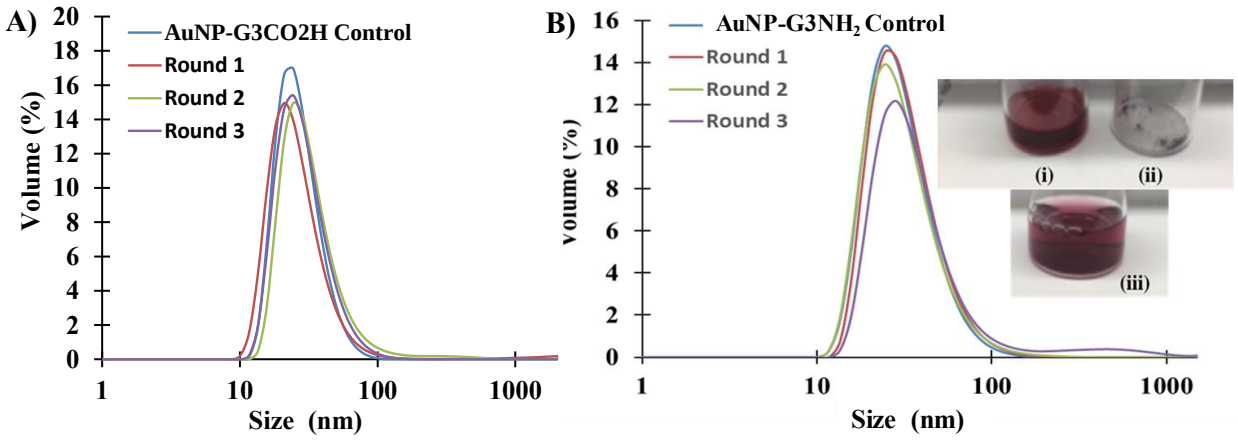

Figure 7. Stability of the dendronized AuNPs towards lyophilization. A) DLS measurements of AuNP-G3CO_2H after three rounds of freeze-dry/dissolution cycles. B) DLS measurements of AuNP-G3NH_2 after three rounds of freeze-dry/dissolution cycles; Inset (i) Starting AuNP-G3NH_2 solution, (ii) Lyophilized AuNP-G3NH_2 powder. (ii) AuNP-G3NH_2 solution after re-suspension after three rounds of freeze-dry cycles.

b) High ionic strength

Before performing the *in vitro* cytotoxicity studies (vide infra), we tested the stability of AuNP-G3CO_2H in 1M NaCl as well as in a more complex salt solution (Hank Buffer) over the course of a week via DLS (Figure 8). We also evaluated the stability of AuNP-G3CO_2H/NH_2 in 1M NaCl (Figure S16b). The results clearly demonstrate that both types of nanoparticles exhibit robust stability in the presence of high ionic strength. It is noteworthy to mention that we did observe some NPs coating on the glass container in the 1M NaCl study after seven days. Nevertheless, this partial deposition of the NPs on glass, due to high ionic concentration, did not cause NPs aggregation in the solution dispersion, as reflected in the DLS data (Figure 8). Moreover, AuNP-G3CO_2H did not show any sign of either aggregation or deposition on glass after 7 days in Hank buffer (Figure 8A). This observation is an important feature since the intravenous administration

(iv) of bio-pharmaceuticals requires the dissolution of our nanoparticles as a stable nano-formulation at cellular osmolality (100 mM NaCl).[45, 46]

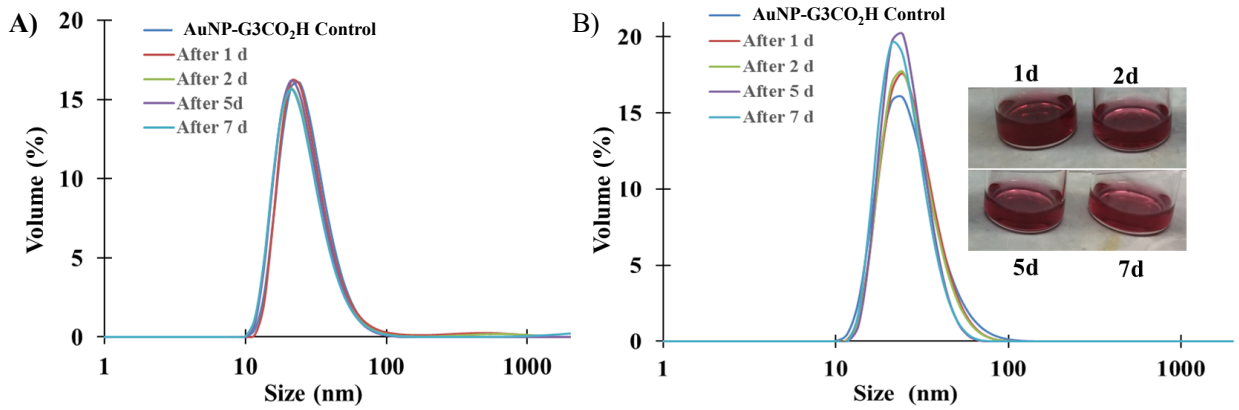

Figure 8. Stability studies of dendronized AuNPs at different ionic strengths. A) DLS measurements of AuNP-G3CO_2H in Hanks Buffer at time intervals 0, 24 h, 48 h, 5 d, 7 d. B) DLS measurements of AuNP-G3CO_2H in 1M NaCl solution at time intervals 0, 24 h, 48 h, 5 d, 7 d; Inset visualization of AuNP-G3CO_2H solution at various time intervals.

c) Biologically relevant media

The dendronized AuNPs were tested in glutathione solution and in serum. In order to assess the stability of our NPs against ligand exchange inside cells,[47] we incubated both AuNP-G3CO_2H and AuNP-G3NH_2 nanoparticles in a 10 mM glutathione solution (intracellular concentration of glutathione[48]). From the DLS measurements in Figure 9A and 9B, it is evident that our dendronized AuNP constructs are very stable over a week-long exposure to 10 mM exogenous glutathione concentration, since neither a reduction in size (which would be the result of exchanging the dendrons with glutathione) or aggregation was observed. Furthermore, our dendronized nanoparticles (AuNP-G3CO_2H) exhibit good stability during incubation in serum at physiological temperature (37^{0}C): the absorption spectra displayed in Figure 9C show very negligible shift of

the surface plasmon resonance (SPR) peak of the AuNPs, which indicates that no aggregation occurred. The gradual decrease in absorbance observed over time in serum is due to a progressive slow deposition of the AuNPs onto the walls of the glass vial: this is mediated by the serum proteins that have a propensity to adsorb on glass surfaces (most likely facilitated at 37 ºC) and can also electrostatically interact with the AuNP ligands. It is noteworthy that the AuNP coating onto glass does stop after 18h in serum, as indicated by the overlap of absorbance between the measurements at 18h and 24h in serum. The stability of AuNP-G3$CO_2H/NH_2$was also tested in serum, and no sign of aggregation was detected, even after 2 days, as shown by the absence of red-shift of the SPR peak of the AuNPs (Figure S26c).

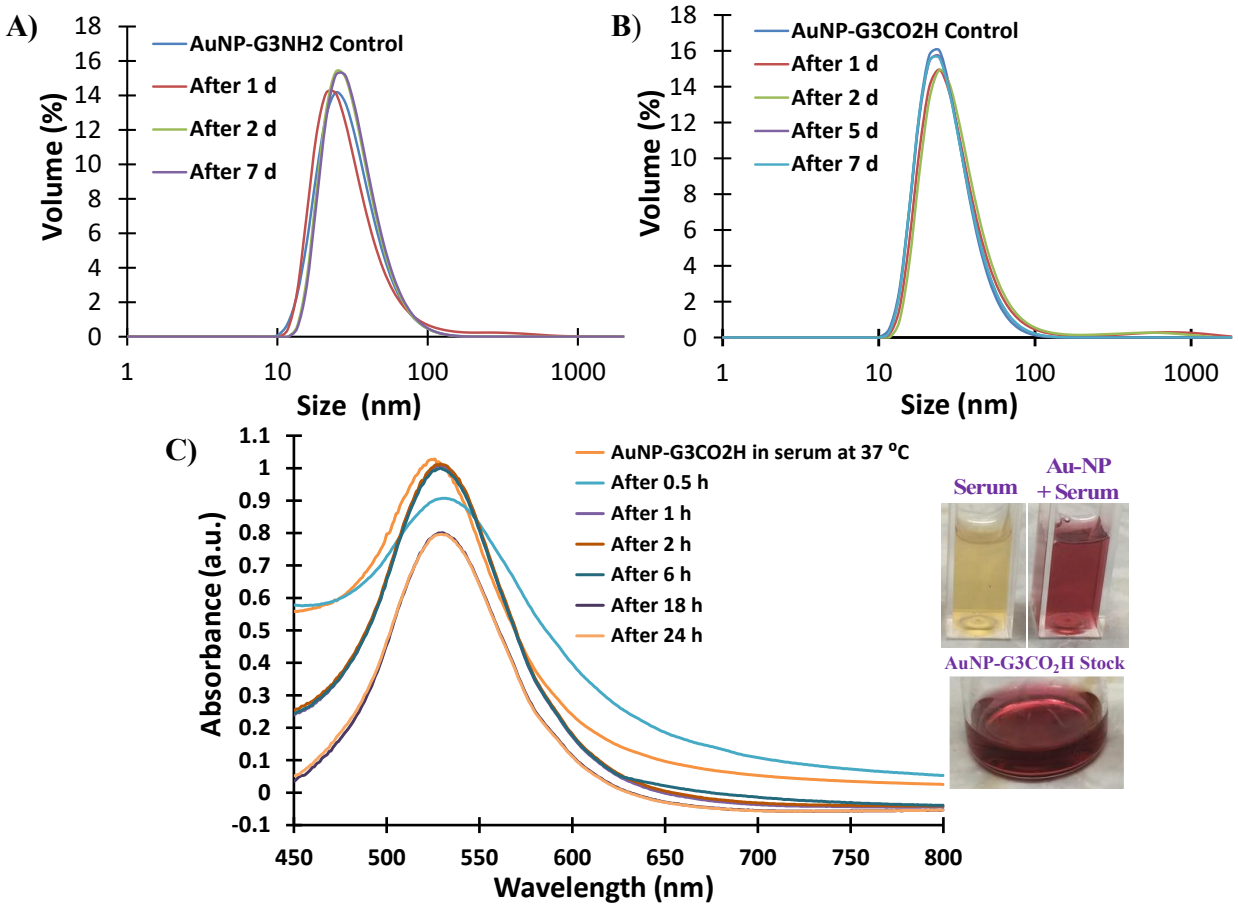

Figure 9. Stability study of AuNP-G3CO_2H in biologically relevant media. A) DLS measurements of AuNP-G3NH_2 in 10 mM glutathione solution at time intervals 0, 1 day, 2 days, 7 days. B) DLS measurements of AuNP-G3CO_2H in 10 mM glutathione solution at time intervals 0, 1 day, 2 days, 7 days; C) UV-vis spectra of AuNP-G3CO_2H in serum at time points 30 min, 1 h, 2 h, 6 h, 18 h, 24 h. Inset: visualization of AuNP-G3CO_2H solution in water (control), serum solution and AuNP-G3CO_2H dissolved in serum after 24 h.

In vitro cytotoxicity studies

Finally, we investigated the toxicity profile of our dendronized nanoparticles as a function of their surface charge. It has been widely reported in literature that positively charged nanoparticles are toxic due to their detrimental interactions with cell membranes, while negatively charged nanoparticles do generally not lead to toxicity.[49, 50] In order to verify the influence of the charge of dendron coating on our AuNPs, we prepared three classes of dendronized nanoparticles and assessed their cytotoxic profile of using MCF-7 cells: a) AuNP-G3CO_2H, b) AuNP-G3NH_2 and c) AuNP-G3CO_2H/NH_2, coated with 60% of TA-TEG-G3CO_2H and 40% of TA-TEG-G3NH_2. From our WST-1 toxicity assay, we observed that indeed the negatively charged AuNP-G3CO_2H nanoparticles were benign up to nanoparticle concentration of 15.6 nM (Fig. 10A). The positively charged AuNP-G3NH_2 nanoparticles were cytotoxic at nanoparticle concentration above 1 nM (Fig. 10B). However, very interestingly, AuNP-G3CO_2H/NH_2 showed a similar toxicity profile to AuNP-G3CO_2H (Fig. 10C) despite the presence of 40% of amino groups on the NPs coating that displayed only a slight overall negative charge (-16.8 mV) at pH 7.5 (Fig. 10D). This result demonstrates the possibility of safely combining dendrons with various end groups in the formulation of multifunctional dendronized nanoparticle constructs.

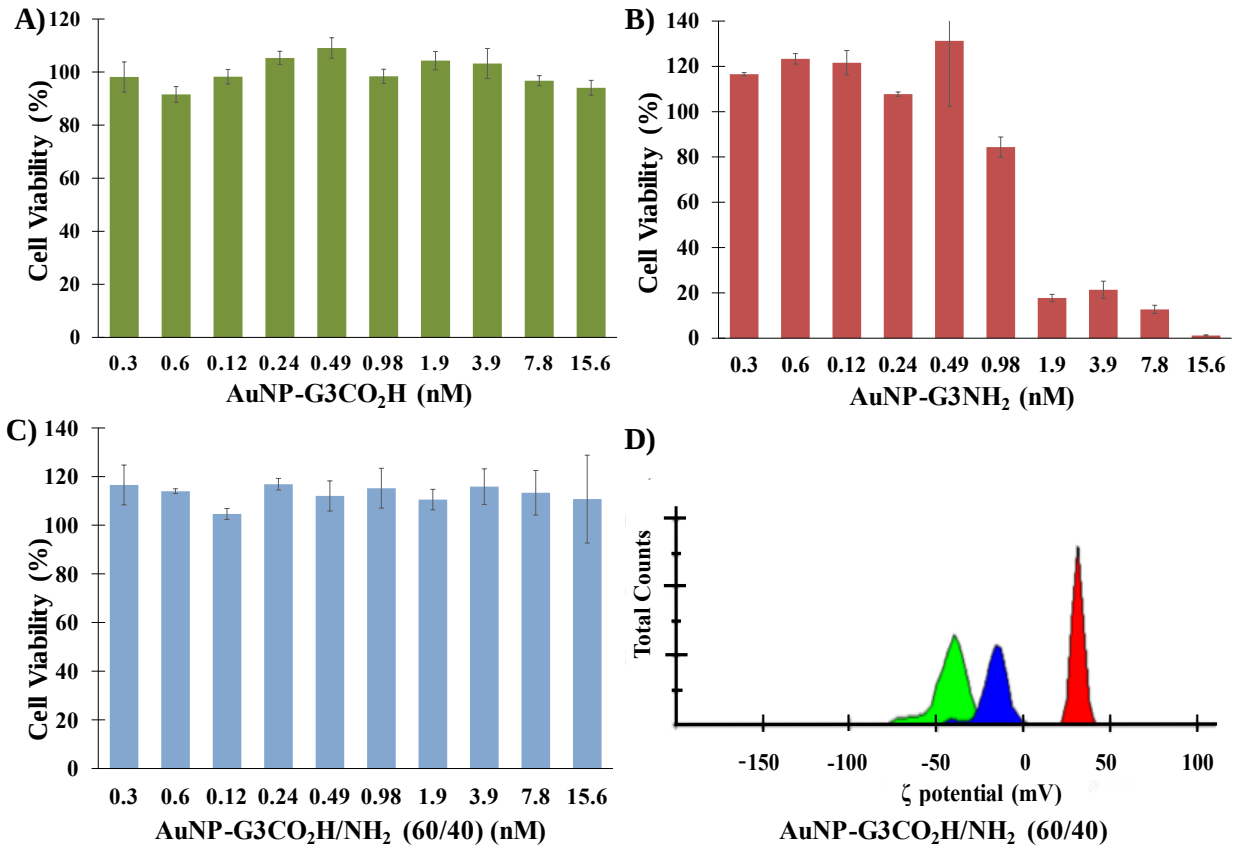

Figure 10. In vitro cytotoxicity studies of dendronized AuNPs. A) Toxicity profile of AuNP-G3CO_2H against MCF-7 breast cancer cell line at NP concentrations ranging from 0.03 nM to 15.6 nM; B) Toxicity profile of AuNP-G3NH_2 at NP concentrations ranging from 0.03 nM to 15.6 nM, C) Toxicity profile of AuNP-G3CO_2H/NH_2 (60/40) at concentrations ranging from 0.03 nM to 15.6 nM; D) Zeta potential measurements of AuNP-G3CO_2H/NH_2 (60/40) at pH 10 (green), 7.5 (blue) and 5.5 (red).

CONCLUSION

In conclusion, we have successfully synthesized a dendritic platform that is both versatile and scalable, and can be used as coating for the formation of extremely stable AuNPs. The two PPI

dendrons prepared herein display either carboxylate or amine termini, which are both easily conjugable functional groups. These can be used either by themselves to create negatively and positively charged AuNPs, respectively, or as a mixed-coating to obtain zwitterionic AuNPs. The branched structure of the dendron allows for a higher density of functional groups at the surface of the nanoparticles (up to 1450 dendrons/NP, equivalent to 11,600 dendritic branches/NP), further contributing to an increase in the overall stability of the AuNPs. This highly dense but thin dendritic monolayer on the AuNPs will allow for optimum payload of biologically relevant entities while maintaining the size and shape requirements for prolonged circulation time *in vivo*. In addition, the dendrons can be conjugated to the payload of interest before or after addition to the AuNPs, which further increase the versatility of the system and can lead to the formation of multifunctional AuNPs. Finally, such system could also be used in the construction of other classes of inorganic NPs due to the robust metal-S bonds conferred via the thioctic acid anchoring moiety.

ASSOCIATED CONTENT

Supporting Information. Materials and Methods section; Protocols ofr the synthesis of spacer intermediates; ^{1}H NMR spectra and ^{13}C NMR spectra of G3CN, TA-TEG-OTs, TA-TEG-G2CN, TA-TEG-G2NH$_2$, TA-TEG-G3CO$_2$Me, TA-TEG-G3CO$_2$H, TA-TEG-G3CN, TA-TEG-G3NH$_2$; ESI spectrum of TA-TEG-G2CN, TA-TEG-G3CO$_2$Me, TA-TEG-G3CO$_2$H, TA-TEG-G3CN; Additional STEM images and zeta potential data of the dendronized AuNPs; Calculation of the maximum theoretical number of thioctic acide ligands per AuNP; Calculation of the experimental number of dendrons per AuNP, using the TGA data; Stability studies of AuNP-G3CO$_2$H/NH$_2$.

The following files are available free of charge: Characterization data (PDF)

AUTHOR INFORMATION

Corresponding Author

*Email address: mdaniel@umbc.edu

Present Addresses

[♯] Center for Nanotechnology, Department of Natural Sciences, Coppin State University, Baltimore, MD 21216, USA.

[Ŧ] Pharmacology & Chemical Biology, Baylor College of Medicine, Houston, TX, USA.

[ǂ] Food and Drug Administration, Silver Spring, MD 20993, USA.

Author Contributions

A.S.R. synthesized and characterized the dendrons, prepared and characterized the dendronized AuNPs, carried out most of the cytotoxicity studies and was primarily responsible for preparing the manuscript. W.E.G. designed and prepared the TA-TEG spacer. P.S.T. contributed to the optimization of TA-TEG-OTs spacer synthesis as well as its coupling to the dendron. B.S. prepared the citrate-coated AuNPs and recorded the TEM images. L.T.D. carried out the stability studies of AuNPs with mixed-coating. Y.J.P. provided the cell cultures and participated in the cytotoxicity studies. W.L. carried out the mass spectrometry analysis of dendron **10**. M.A.K. supervised the mass spectrometry data acquisition. P.S. supervised the cytotoxicity studies. M.C.D. conceived the experiments and supervised the synthesized and characterization of the dendrons and of the dendronized AuNPs. A.S.R. and M.C.D. contributed to data interpretation.

Funding Sources

NSF (CHE1507462), NIH (T32GM066706) as well as UMBC URA awards.

ACKNOWLEDGMENT

The authors are grateful for the financial support from NSF (CHE1507462), NIH (T32GM066706). They would also like to acknowledge Josh Wilhide (MCAC, UMBC), for assistance in acquisition of HRMS spectra. They are also thankful to Tagide deCarvalho for her assistance in sample preparation and acquisition of TEM images, as well to Laszlo Takacs for his assistance in acquisition of STEM images. Additional support was provided by the University of Maryland School of Pharmacy Mass Spectrometry Center (SOP1841-IQB2014).

REFERENCES

1. Ferrari, M., Cancer nanotechnology: opportunities and challenges. *Nat Rev Cancer* **2005,** *5* (3), 161-71.
2. Sanhai, W. R.; Sakamoto, J. H.; Canady, R.; Ferrari, M., Seven challenges for nanomedicine. *Nat Nanotechnol* **2008,** *3* (5), 242-4.
3. Allen, T. M.; Cullis, P. R., Drug delivery systems: entering the mainstream. *Science* **2004,** *303* (5665), 1818-22.
4. Lajunen, T.; Kontturi, L. S.; Viitala, L.; Manna, M.; Cramariuc, O.; Róg, T.; Bunker, A.; Laaksonen, T.; Viitala, T.; Murtomäki, L.; Urtti, A., Indocyanine Green-Loaded Liposomes for Light-Triggered Drug Release. *Mol Pharm* **2016,** *13* (6), 2095-107.
5. Perrie, Y., Gregory Gregoriadis: Introducing liposomes to drug delivery. *J Drug Target* **2008,** *16* (7), 518-9.
6. Menjoge, A. R.; Kannan, R. M.; Tomalia, D. A., Dendrimer-based drug and imaging conjugates: design considerations for nanomedical applications. *Drug Discov Today* **2010,** *15* (5-6), 171-85.
7. Parat, A.; Bordeianu, C.; Dib, H.; Garofalo, A.; Walter, A.; Bégin-Colin, S.; Felder-Flesch, D., Dendrimer-nanoparticle conjugates in nanomedicine. *Nanomedicine (Lond)* **2015,** *10* (6), 977-92.
8. Same, S.; Aghanejad, A.; Akbari Nakhjavani, S.; Barar, J.; Omidi, Y., Radiolabeled theranostics: magnetic and gold nanoparticles. *Bioimpacts* **2016,** *6* (3), 169-181.

9. Frosina, G., Nanoparticle-mediated drug delivery to high-grade gliomas. *Nanomedicine* **2016,** *12* (4), 1083-93.
10. Singh, T. G.; Dhiman, S. In *Nanocarriers as nanomedicine: a promising platform for drug delivery in nanopharmaceuticals*, CRC Press: 2016; pp 590-599.
11. Ashford, M. In *Development and commercialization of nanocarrier-based drug products*, Wiley-VCH Verlag GmbH & Co. KGaA: 2017; pp 697-734.
12. Basha, M., Nanotechnology as a Promising Strategy for Anticancer Drug Delivery. *Curr. Drug Delivery* **2018,** *15* (4), 497-509.
13. Peer, D.; Karp, J. M.; Hong, S.; Farokhzad, O. C.; Margalit, R.; Langer, R., Nanocarriers as an emerging platform for cancer therapy. *Nat Nanotechnol* **2007,** *2* (12), 751-60.
14. Majoros, I. J.; Myc, A.; Thomas, T.; Mehta, C. B.; Baker, J. R., PAMAM dendrimer-based multifunctional conjugate for cancer therapy: synthesis, characterization, and functionality. *Biomacromolecules* **2006,** *7* (2), 572-9.
15. Lim, J.; Simanek, E., Triazine dendrimers as drug delivery systems: From synthesis to therapy. *Advanced Drug Delivery Reviews* **2012,** *64* (9), 826-835.
16. Thakor, A. S.; Jokerst, J.; Zavaleta, C.; Massoud, T. F.; Gambhir, S. S., Gold nanoparticles: a revival in precious metal administration to patients. *Nano Lett* **2011,** *11* (10), 4029-36.
17. Kaufman, E. A.; Tarallo, R.; Elacqua, E.; Carberry, T. P.; Weck, M., Synthesis of Well-Defined Bifunctional Newkome-Type Dendrimers. *Macromolecules* **2017,** *50* (13), 4897-4905.
18. Brazzale, C.; Mastrotto, F.; Moody, P.; Watson, P. D.; Balasso, A.; Malfanti, A.; Mantovani, G.; Caliceti, P.; Alexander, C.; Jones, A. T.; Salmaso, S., Control of targeting ligand display by pH-responsive polymers on gold nanoparticles mediates selective entry into cancer cells. *Nanoscale* **2017,** *9* (31), 11137-11147.
19. Lee, C. C.; MacKay, J. A.; Fréchet, J. M.; Szoka, F. C., Designing dendrimers for biological applications. *Nat Biotechnol* **2005,** *23* (12), 1517-26.
20. Bolhassani, A.; Javanzad, S.; Saleh, T.; Hashemi, M.; Aghasadeghi, M. R.; Sadat, S. M., Polymeric nanoparticles: potent vectors for vaccine delivery targeting cancer and infectious diseases. *Hum Vaccin Immunother* **2014,** *10* (2), 321-32.
21. Gillies, E. R.; Fréchet, J. M., Dendrimers and dendritic polymers in drug delivery. *Drug Discov Today* **2005,** *10* (1), 35-43.
22. Brunetti, V.; Bouchet, L. M.; Strumia, M. C., Nanoparticle-cored dendrimers: functional hybrid nanocomposites as a new platform for drug delivery systems. *Nanoscale* **2015,** *7* (9), 3808-3816.
23. Shon, Y.; Choi, D.; Dare, J.; Dinh, T., Synthesis of nanoparticle-cored dendrimers by convergent dendritic functionalization of monolayer-protected nanoparticles. *Langmuir* **2008,** *24* (13), 6924-6931.
24. Daniel, M.; Grow, M.; Pan, H.; Bednarek, M.; Ghann, W.; Zabetakis, K.; Cornish, J., Gold nanoparticle-cored poly(propyleneimine) dendrimers as a new platform for multifunctional drug delivery systems. *New Journal of Chemistry* **2011,** *35* (10), 2366-2374.
25. Cho, T. J.; Zangmeister, R. A.; MacCuspie, R. I.; Patri, A. K.; Hackley, V. A., Newkome-Type Dendron-Stabilized Gold Nanoparticles: Synthesis, Reactivity, and Stability. *Chem. Mater.* **2011,** *23* (10), 2665-2676.
26. Bordeianu, C.; Parat, A.; Piant, S.; Walter, A.; Zbaraszczuk-Affolter, C.; Meyer, F.; Begin-Colin, S.; Boutry, S.; Muller, R. N.; Jouberton, E.; Chezal, J. M.; Labeille, B.; Cinotti, E.; Perrot, J. L.;

Miot-Noirault, E.; Laurent, S.; Felder-Flesch, D., Evaluation of the Active Targeting of Melanin Granules after Intravenous Injection of Dendronized Nanoparticles. *Mol. Pharmaceutics* **2018,** *15* (2), 536-547.

27. Deol, S.; Weerasuriya, N.; Shon, Y.-S., Stability, cytotoxicity and cell uptake of water-soluble dendron-conjugated gold nanoparticles with 3, 12 and 17 nm cores. *J. Mater. Chem. B* **2015,** *3* (29), 6071-6080.

28. Enciso, A. E.; Doni, G.; Nifosì, R.; Palazzesi, F.; Gonzalez, R.; Ellsworth, A. A.; Coffer, J. L.; Walker, A. V.; Pavan, G. M.; Mohamed, A. A.; Simanek, E. E., Facile synthesis of stable, water soluble, dendron-coated gold nanoparticles. *Nanoscale* **2017,** *9* (9), 3128-3132.

29. Pan, H.; Grow, M. E.; Wilson, O.; Daniel, M.-C., A new poly(propylene imine) dendron as potential convenient building-block in the construction of multifunctional systems. *Tetrahedron* **2013,** *69* (13), 2799-2806.

30. Haiss, W.; Thanh, N. T.; Aveyard, J.; Fernig, D. G., Determination of size and concentration of gold nanoparticles from UV-vis spectra. *Anal Chem* **2007,** *79* (11), 4215-21.

31. Ghann, W.; Aras, O.; Fleiter, T.; Daniel, M., Syntheses and Characterization of Lisinopril-Coated Gold Nanoparticles as Highly Stable Targeted CT Contrast Agents in Cardiovascular Diseases. *Langmuir* **2012,** *28* (28), 10398-10408.

32. Tournebize, J.; Boudier, A.; Sapin-Minet, A.; Maincent, P.; Leroy, P.; Schneider, R., Role of Gold Nanoparticles Capping Density on Stability and Surface Reactivity to Design Drug Delivery Platforms. *ACS Appl. Mater. Interfaces* **2012,** *4* (11), 5790-5799.

33. Roux, S.; Garcia, B.; Bridot, J.-L.; Salome, M.; Marquette, C.; Lemelle, L.; Gillet, P.; Blum, L.; Perriat, P.; Tillement, O., Synthesis, Characterization of Dihydrolipoic Acid Capped Gold Nanoparticles, and Functionalization by the Electroluminescent Luminol. *Langmuir* **2005,** *21* (6), 2526-2536.

34. Buhleier, E.; Wehner, W.; Voegtle, F., "Cascade"- and "nonskid-chain-like" syntheses of molecular cavity topologies. *Synthesis* **1978,** (2), 155-8.

35. van Duijvenbode, R. C.; Rajanayagam, A.; Koper, G. J. M.; Baars, M. W. P. L.; de Waal, B. F. M.; Meijer, E. W.; Borkovec, M., Synthesis and Protonation Behavior of Carboxylate-Functionalized Poly(propyleneimine) Dendrimers. *Macromolecules* **2000,** *33* (1), 46-52.

36. Hendry, D.; Hough, L.; Richardson, A. C., Enantiospecific synthesis of (6R,7S,8aR)-dihydroxyindolizidine and (6R,7R,8S,8aR)-trihydroxyindolizidine from D-glucose. *Tetrahedron Lett.* **1987,** *28* (39), 4601-4.

37. Ojea-Jimenez, I.; Puntes, V., Instability of Cationic Gold Nanoparticle Bioconjugates: The Role of Citrate Ions. *J. Am. Chem. Soc.* **2009,** *131* (37), 13320-13327.

38. Chou, L. Y.; Chan, W. C., Fluorescence-tagged gold nanoparticles for rapidly characterizing the size-dependent biodistribution in tumor models. *Adv Healthc Mater* **2012,** *1* (6), 714-21.

39. Hinterwirth, H.; Kappel, S.; Waitz, T.; Prohaska, T.; Lindner, W.; Laemmerhofer, M., Quantifying Thiol Ligand Density of Self-Assembled Monolayers on Gold Nanoparticles by Inductively Coupled Plasma-Mass Spectrometry. *ACS Nano* **2013,** *7* (2), 1129-1136.

40. Wang, F.; Wang, Y.-C.; Dou, S.; Xiong, M.-H.; Sun, T.-M.; Wang, J., Doxorubicin-Tethered Responsive Gold Nanoparticles Facilitate Intracellular Drug Delivery for Overcoming Multidrug Resistance in Cancer Cells. *ACS Nano* **2011,** *5* (5), 3679-3692.

41. Tsai, D.; Cho, T.; Elzey, S.; Gigault, J.; Hackley, V., Quantitative analysis of dendron-conjugated cisplatin-complexed gold nanoparticles using scanning particle mobility mass spectrometry. *Nanoscale* **2013,** *5* (12), 5390-5395.
42. Cho, T. J.; MacCuspie, R. I.; Gigault, J.; Gorham, J. M.; Elliott, J. T.; Hackley, V. A., Highly Stable Positively Charged Dendron-Encapsulated Gold Nanoparticles. *Langmuir* **2014,** *30* (13), 3883-3893.
43. Alkilany, A. M.; Abulateefeh, S. R.; Mills, K. K.; Bani Yaseen, A. I.; Hamaly, M. A.; Alkhatib, H. S.; Aiedeh, K. M.; Stone, J. W., Colloidal Stability of Citrate and Mercaptoacetic Acid Capped Gold Nanoparticles upon Lyophilization: Effect of Capping Ligand Attachment and Type of Cryoprotectants. *Langmuir* **2014,** *30* (46), 13799-13808.
44. Gupta, A.; Moyano, D. F.; Parnsubsakul, A.; Papadopoulos, A.; Wang, L.-S.; Landis, R. F.; Das, R.; Rotello, V. M., Ultrastable and Biofunctionalizable Gold Nanoparticles. *ACS Appl. Mater. Interfaces* **2016,** *8* (22), 14096-14101.
45. Min, Y.; Caster, J. M.; Eblan, M. J.; Wang, A. Z., Clinical Translation of Nanomedicine. *Chem. Rev. (Washington, DC, U. S.)* **2015,** *115* (19), 11147-11190.
46. Satalkar, P.; Elger, B. S.; Hunziker, P.; Shaw, D., Challenges of clinical translation in nanomedicine: A qualitative study. *Nanomedicine (N. Y., NY, U. S.)* **2016,** *12* (4), 893-900.
47. Hong, R.; Han, G.; Fernandez, J. M.; Kim, B.-j.; Forbes, N. S.; Rotello, V. M., Glutathione-Mediated Delivery and Release Using Monolayer Protected Nanoparticle Carriers. *J. Am. Chem. Soc.* **2006,** *128* (4), 1078-1079.
48. Montero, D.; Tachibana, C.; Rahr Winther, J.; Appenzeller-Herzog, C., Intracellular glutathione pools are heterogeneously concentrated. *Redox Biol.* **2013,** *1* (1), 508-513.
49. Alkilany, A. M.; Murphy, C. J., Toxicity and cellular uptake of gold nanoparticles: what we have learned so far? *J. Nanopart. Res.* **2010,** *12* (7), 2313-2333.
50. Frohlich, E., The role of surface charge in cellular uptake and cytotoxicity of medical nanoparticles. *Int J Nanomedicine* **2012,** *7*, 5577-91.

Table of Content